

Supporting Information

Muratore et al. 10.1073/pnas.1119817109

SI Text

An in silico procedure based on FLAP (fingerprints for ligands and proteins) software (1, 2) was used to perform a structure-based virtual screening for the selection of candidate inhibitors of the PA–PB1 interaction. FLAP is a screening program based on 3D-molecular similarity and has been successfully used on both structure-based and ligand-based projects (3–5). The FLAP algorithm functions by superimposing test molecules onto one or more templates, that can be proteins or other molecules, and by measuring common molecular interaction field (MIF) overlaps (2). Scoring functions are used to obtain a similarity ranking of the test molecules on the basis of the MIF volume overlap. Here, the aim was to search small molecule compounds having high affinity for the PA–PB1 interaction site. The crystallographic structure of a large C-terminal fragment of PA (amino acids 257–716) bound to a PB1-derived peptide (Protein Data Bank, PDB, code 3CM8) (6) was modified by removing the PB1 moiety. FLAP automatically identified the formed cavity in the PA subunit and described the cavity in terms of molecular interaction fields from GRID force field (7). Taking into account that the PA subunit might assume different conformations in a nonbound state, six additional snapshots of the PA subunit extracted from the 3CM8 structure were created (Fig. S14) using the molecular dynamic (MD) protocol in AMBER software inside Sybyl suite. Thus, seven cavities from the PA conformations were then used as templates for structure-based virtual screening. A comparative analysis of the cavities for the seven PA conformations showed that the shape and volume can significantly mutate (Fig. S1B) and that the smallest cavity belongs to the PA crystal structure template (PDB code 3CM8), which corresponds to the conformation bound to PB1. A selection of 3 million compounds from the ZINC database was used for virtual screening and the first 4,000 top ranked compounds were selected. The compounds were then filtered by absorption, distribution, metabolism, and excretion (ADME) properties to avoid those compounds having a too low or a too high solubility, as well as too flexible or highly charged compounds. In total, 293 compounds showed good ADME properties and high similarity scores for the majority of the protein cavity snapshots. Among the 293 compounds, 32 molecules were selected according to their availability, cost, and drugability. Details on computational methods are given in *SI Materials and Methods*.

SI Materials and Methods

Computational Methods. Molecular dynamics simulations. The crystal structure of the PA–PB1 complex of FluA virus (PDB code 3CM8) was used as the initial structure of our simulation. Molecular dynamics (MD) simulations were performed to obtain dynamic structural information about the PA cavity using Sybyl package. The aim was to build a dynamic PA pharmacophoric model to describe the dynamic interaction features of the protein–protein complex more accurately than using the static crystal structure. All of the calculations of energy minimization and system equilibration protocols were performed with the AMBER suite through Sybyl interface. To keep the whole system neutral, Cl-counterions were added and then solvated using water molecules around the complex. The system was annealed from 0 to 300 K over a period of 20 ps and equilibrated for 20 ps at a temperature of 300 K, then again equilibrated for 200 ps, while maintaining the force constants on the restrained atoms. The final phase of the simulation was run under the same conditions for a total of 3 ns. Each of the MD snapshots extracted using normal-mode analysis was submitted to FLAP analysis to

find the surface binding pockets and the corresponding protein-snapshot pharmacophoric features. The procedure was repeated for all of the protein snapshots and the single pharmacophoric features were collected in a unique global “dynamic pharmacophore” model. Finally, the global pharmacophore was used as a template in a virtual screening for compounds selection.

Virtual screening. The crystal structure 3CM8 and the six conformations were used as templates for structure-based virtual screening using FLAP software. A ZINC compound library of trusted vendors was used for screening. The GRID (7, 8) probes defining shape (H), hydrophobic interactions (DRY), H-bond donor (N1), and H-bond acceptor interactions were used to generate the molecular interaction fields and evaluate the similarity between the screened compounds and the protein cavities. VolSurf+ software (9) was then used to filter the best 4,000 compounds by ADME properties.

Homology model. Comparative modeling of FluB was performed using FluA as a structural template. The sequence of FluB was aligned to FluA using ClustalW (10) with standard settings as implemented in Jalview 2.6.1 (11). Modeller (12) was then used to mutate the structural template into FluB, according to the sequence alignment, and the structure optimized using spatial restraints to best fit the FluA template crystallographic coordinates.

Compounds and Peptides. Ribavirin (RBV; 1-D-ribofuranosyl-1,2,4-triazole-3-carboxamide) and oseltamivir carboxylic acid, the active form of oseltamivir [(3R,4R,5S)-4-acetamido-5-amino-3-(1-ethyl-propoxy)-1-cyclohexene-1-carboxylic acid] were obtained from Roche. Ganciclovir (GCV) and amantadine were purchased from Sigma. Test compounds were purchased from SPECS, Chembridge, and VITAS-M and dissolved in dimethyl sulfoxide (DMSO).

The PB1_{1–15} and PB1_{1–15}–Tat peptides were synthesized and purified by the Peptide Facility of CRIBI Biotechnology Center (University of Padua, Padua, Italy). The PB1_{1–15}–Tat peptide possesses a C-terminal sequence from the HIV Tat protein (amino acids 47–59), which has been shown to mediate cell entry (13). A scrambled peptide consisting of the same amino acid composition as the PB1_{1–15} peptide but with the order randomized was purchased from Sigma. The peptide corresponding to the last 22 residues of HCMV UL54 was synthesized as described (14). All peptides were dissolved in water.

Plasmids. Plasmids pcDNA–PB1, pcDNA–PB2, pcDNA–PA, and pcDNA–NP, containing cDNA copies of the influenza A/PR/8/34 PB1, PB2, PA, and NP genes, respectively, were created as described elsewhere (15). Plasmid pPoll–Flu–ffLuc, which contains an influenza virus-based luciferase minireplicon vRNA under the control of the human RNA polymerase I promoter (16), was provided by L. Tiley (University of Cambridge, Cambridge, UK). Plasmid pRL–SV40 expressing the *Renilla* luciferase was purchased from Promega. Plasmids pCI–PB1, pCI–PB2, pCI–PA, and pCI–NP, expressing B/Panama/45/90 polymerase and NP proteins (17), and plasmid pPoll–HA–GFP, which contains an influenza virus-based green fluorescent protein (GFP) minireplicon vRNA under the control of the human RNA polymerase I promoter, were a gift of W. S. Barclay (Imperial College, London, UK). The pcDNA–PA–GFP plasmid, which encodes a PA–GFP fusion protein (18), was kindly provided by E. Fodor (University of Oxford, Oxford, UK). To generate the pET28a–PA_{239–716} plasmid, which encodes a 6His–PA_{239–716} fusion protein, PA coding sequence was amplified from pcDNA–PA by PCR with primers 5′-TTTATGAATTCAACGGCTA-

CATTGAGGGC-3' and 5'-TAAAGCGGCCCTAACTCA-ATGCATGTGT-3' and cloned into the EcoRI/NotI sites of pET28a (Novagen). To obtain plasmid pD15-PB1₁₋₂₅, the DNA sequence encoding the first 25 residues of PB1 was amplified from pcDNA-PB1 plasmid with primers 5'-AAAAAAGCTCGA-GATGGATGTCATCCGACC-3' and 5'-TAAAAAAGCGGCTCTAGGTATAAGGAAAGTC-3' and cloned into the XhoI/MluI sites of pD15-GST (19). Both expression plasmids were sequenced to verify correctness of the constructs and the absence of undesired mutations.

Cells and Viruses. Human embryonic kidney (HEK) 293T, Madin-Darby Canine Kidney (MDCK), human lung carcinoma (A549), African Green Monkey kidney (Vero), mouse fibroblast (L929), human laryngeal carcinoma (HEp-2), and human foreskin fibroblast (HFF) cells were maintained in DMEM (Life Biotechnologies) supplemented with 10% (vol/vol) FBS (Life Biotechnologies). All cells were grown in the presence of 100 units/mL penicillin and 100 µg/mL streptomycin (Life Biotechnologies) and were maintained at 37 °C in a humidified atmosphere supplemented with 5% CO₂.

Influenza A/PR/8/34 virus (H1N1, Cambridge lineage) was obtained from the Division of Virology's (Department of Pathology, University of Cambridge, Cambridge, United Kingdom) collection of influenza viruses. The FluA viruses A/Wisconsin/67/05 and A/Solomon Island/3/06, and influenza B/Malaysia/2506/4 virus were provided by R. Cusinato (Clinical Microbiology and Virology Unit, Padua University Hospital, Padua, Italy); influenza B/Lee/40 virus was obtained from W. S. Barclay (Imperial College, London, United Kingdom). The clinical isolates A/Roma-ISS/2/08 and A/Parma/24/09 were kindly provided by I. Donatelli (Istituto Superiore di Sanità, Rome, Italy); local strains of the new pandemic variant H1N1 FluA virus (A/Padova/30/2011, A/Padova/72/2011, and A/Padova/253/2011) and of FluB virus (B/Padova/2/2011, B/Padova/3/2011, and B/Padova/42/2011) were provided by C. Salata and A. Calistri (University of Padua, Padua, Italy). All influenza viruses were propagated in MDCK cells. Herpes simplex virus type 1 (HSV-1, strain F) and human cytomegalovirus (HCMV, strain AD169) were purchased from the American Type Culture Collection. Vesicular stomatitis virus (VSV) was provided by G. Gribaudo (University of Turin, Turin, Italy). Clinical isolates of human measles virus (MV), coxsackie virus B1 (COX B1), respiratory syncytial virus (RSV), and adenovirus (AdV) were collected at the Microbiology and Virology Unity of Padua University Hospital.

Protein Expression and Purification. *Escherichia coli*-expressed, purified GST, and GST-Ubc9 (a fusion between GST and Ubc9, the cellular SUMO-conjugating E2 enzyme) proteins were obtained as previously described (19).

To obtain the 6His-PA₂₃₉₋₇₁₆ protein, the pET28a-PA₂₃₉₋₇₁₆ plasmid was transformed into *E. coli* strain BL21(DE3)pLysS (Stratagene). Typically, cells were grown in Luria Bertani (LB) medium containing 50 µg/mL kanamycin until the OD₆₀₀ was 0.8 and then induced by the addition of 0.5 mM isopropyl-β-D-thiogalactopyranoside (IPTG, ICN) overnight (O/N) at 16 °C. Cells were pelleted, resuspended in 20 mM Tris-HCl pH 8.0, 500 mM NaCl, 500 mM urea, 10 mM β-mercaptoethanol, 25 mM imidazole, 1 mg/mL lysozyme, and complete protease inhibitors (Roche Molecular Biochemicals), and then lysed by two freeze/thaw cycles and by sonication. The lysate was centrifuged at 16,000 × g for 30 min, applied to a 0.5-mL Ni-NTA agarose resin column (Qiagen) that had been equilibrated in resuspension buffer. Protein was eluted with 20 mM Tris-HCl pH 8.0, 500 mM NaCl, 500 mM urea, 10 mM β-mercaptoethanol, and 250 mM imidazole.

The GST-PB1₁₋₂₅ fusion protein was purified from *E. coli* BL21 (DE3)pLysS harboring the pD15-PB1₁₋₂₅ plasmid. Cells were grown in LB medium containing 100 µg/mL ampicillin until the OD₆₀₀ was 0.8 and then induced by the addition of 0.5 mM IPTG O/N at 16 °C. Cells were pelleted, resuspended in 50 mM Tris-HCl pH 8.0, 150 mM

NaCl, 20% (vol/vol) glycerol, 5 mM DTT, 1 mg/mL lysozyme, and complete protease inhibitors, and then lysed by two freeze/thaw cycles followed by sonication. The lysate was centrifuged at 16,000 × g for 30 min, applied to a 0.5-mL glutathione-sepharose 4 FastFlow column (Amersham Pharmacia Biotech) that had been equilibrated in lysis buffer. Finally, protein was eluted with 50 mM Tris-HCl pH 8.0, 150 mM NaCl, 20% (vol/vol) glycerol, 5 mM DTT, and glutathione 40 mM. Both 6His-PA₂₃₉₋₇₁₆ and GST-PB1₁₋₂₅ purified proteins were dialyzed against 20 mM Tris-HCl pH 8.0, 150 mM NaCl, 30% (vol/vol) glycerol, 5 mM DTT and stored at -80 °C.

PA-PB1 Interaction ELISA. Microtiter plates (Nuova Aptca) were coated with 400 ng of purified 6His-PA₂₃₉₋₇₁₆ for 3 h at 37 °C and then blocked with 2% (wt/vol) BSA (Sigma) in phosphate buffer saline (PBS) for 1 h. After washes with PBS containing 0.3% Tween 20, 200 ng of GST-PB1₁₋₂₅, GST-Ubc9, or GST alone were added and incubated O/N at room temperature (RT) in the absence or the presence of test compounds or PB1₁₋₁₅-Tat peptide. After washing, samples were incubated with horseradish peroxidase (HRP)-conjugated anti-GST monoclonal antibody [GenScript; diluted 1:3,000 in PBS containing 2% (vol/vol) FBS]. Following washes with PBS plus 0.3% Tween 20, the chromogenic substrate 3,3',5,5'-tetramethylbenzidine (TMB) (KPL) was added and absorbance was read at 450 nm on an ELISA plate reader (Tecan Sunrise).

His-Pulldown Assay. PB1 was translated in vitro from pcDNA-PB1 plasmid by using the TNT T7 coupled reticulocyte lysate system (Promega) according to the manufacturer's suggestion and labeled with [³⁵S]-methionine (PerkinElmer). Purified 6His-PA₂₃₉₋₇₁₆ protein (1 µg) was incubated with 25 µL of in vitro translated PB1 O/N at RT in binding buffer (20 mM Tris-HCl pH 8, 150 mM NaCl, 5 mM DTT) containing 2.5 µL of RNase-It RNase Mixture (Stratagene) and 25 units of benzonase (Sigma) in the presence of 200 µM of test compounds or PB1₁₋₁₅-Tat peptide, or DMSO as a control. The binding reactions were then loaded onto 0.1-mL Ni-NTA agarose resin columns. The columns were washed with 1 mL of wash buffer (20 mM Tris-HCl pH 8, 150 mM NaCl, 5 mM DTT, 2% (vol/vol) Nonidet P-40, and 2% (vol/vol) Triton X-100). Bound proteins were then eluted with binding buffer containing 250 mM imidazole and visualized by SDS-polyacrylamide gel electrophoresis (SDS/PAGE) and autoradiography.

Cytotoxicity Assay. The cytotoxicities of test compounds were assayed by the 3-(4,5-dimethylthiazol-2-yl)-2,5-diphenyl tetrazolium bromide (MTT) method as described (20).

Analysis of Nuclear Accumulation of the PA-PB1 Complex. HEK 293T cells were transiently transfected using the Arrest-IN (Biosystems) with pcDNA-PA-GFP and pcDNA-PB1 in the absence or the presence of test compounds. At 24 h posttransfection, cells were fixed for 20 min with 4% (vol/vol) formaldehyde in PBS. After permeabilization with 0.2% Triton X-100 in PBS for 5 min at RT, cells were incubated for 20 min with TOTO-3 iodide (Molecular Probes) in PBS and 4% (vol/vol) FBS, mounted using mounting fluid [70% (vol/vol) glycerol in PBS], and imaged using a Leica TCS-NT/SP2 confocal microscope equipped with a 63× oil immersion objective. Images were digitally analyzed with Leica software.

For analysis of PA localization in infected cells, MDCK cells were seeded at 2 × 10⁵ per well on glass coverslips in 24-well plates. The next day, cells were infected with PR8 at a multiplicity of infection (MOI) of 2 in the presence of the test compounds or DMSO. At 6 h p.i., cells were fixed and then permeabilized as described above. After washing with PBS, cells were incubated with a primary rabbit anti-PA antibody (21); bound antibody was then detected by a secondary goat antirabbit fluorescein-conjugated antibody (Ig-FITC, Chemicon International) at a dilution of 1:100 for 1 h at 37 °C. Samples were then analyzed by confocal laser microscopy as described above.

Minireplicon Assays. For FluA virus minireplicon assays, HEK 293T cells were seeded into 24-well plates at a density of 2×10^5 cells per well and incubated O/N at 37 °C. Cells were then cotransfected with pcDNA–PB1, pcDNA–PB2, pcDNA–PA, pcDNA–NP plasmids, with the influenza virus-specific RNA polymerase I-driven firefly luciferase reporter plasmid (pPolI–Flu–ffLuc), and with pRL–SV40 plasmid (coding for *Renilla* luciferase), which served to normalize variations in transfection efficiency. Transfections were performed with Arrest-IN (Biosystems) according to the manufacturer's recommendations in the presence of the test compounds, PB1_{1–15}–Tat peptide, or DMSO. Cell medium was replaced 5 h posttransfection with DMEM containing compounds, PB1_{1–15}–Tat peptide, or DMSO. At 24 h posttransfection, cells were harvested and both firefly luciferase and *Renilla* luciferase expression were determined using the Dual Luciferase Assay kit from Promega. The activity measured in control transfection reactions containing DMSO was set at 100%.

For FluB virus minireplicon assays, HEK 293T cells were cotransfected with pCI–PB1, pCI–PB2, pCI–PA, pCI–NP plasmids and with the pPolI–HA–GFP reporter plasmid expressing RNA polymerase I-driven GFP. Transfections were performed in the presence of the test compounds or DMSO as described above. Cell medium was replaced 5 h posttransfection with DMEM containing compounds or DMSO. At 24 h posttransfection, cells were fixed for 20 min with 4% (vol/vol) formaldehyde in PBS and then permeabilized with 0.2% Triton X-100 in PBS for 5 min at RT. Cells were then incubated for 20 min with TOTO-3 iodide (Molecular Probes) in PBS and 4% (vol/vol) FBS, and imaged by confocal microscopy as described above.

Antiviral Assays with Influenza Viruses. For plaque reduction assays (PRA) with FluA and FluB viruses, MDCK cells were seeded at a density of 5×10^5 cells per well in 12-well plates. The next day, cells were infected with the FluA or FluB virus at 40 pfu per well in DMEM plus 0.14% BSA and 1 µg/mL TPCK-treated trypsin (Worthington Biochemical) for 1 h at 37 °C. Cells were then incubated with medium containing 1.2% (wt/vol) Avicel cellulose, 0.14% BSA, 1 µg/mL TPCK-treated trypsin, and various concentrations of each test compound. After 2 d, cell monolayers were fixed with 4% (vol/vol) formaldehyde and stained with 0.1% toluidine blue, and plaques were counted.

For virus yield reduction assays, MDCK cells were seeded at a density of 2×10^5 cells per well in 24-well plates and incubated O/N. The next day, cells were infected with influenza A/PR/8/34 virus at an

MOI of 0.01 in DMEM plus 0.14% BSA, and 1 µg/mL TPCK-treated trypsin for 1 h at 37 °C. Cells were then incubated with medium containing 0.14% BSA, 1 µg/mL TPCK-treated trypsin, and various concentrations of each compound. At 12 and 48 h post-infection (p.i.), cell culture supernatants were collected and viral progeny was titrated by plaque assays on fresh MDCK monolayers.

Analysis of Viral Protein Synthesis. MDCK cells were seeded at 2×10^5 cells per well in 24-well plates. The next day, cells were infected with influenza A/PR/8/34 virus at an MOI of 5 in DMEM plus 0.14% BSA and 1 µg/mL TPCK-treated trypsin for 1 h at 37 °C. Cells were then incubated with medium containing 0.14% BSA, 1 µg/mL TPCK-treated trypsin, and various concentrations of each test compound. After 12 h, cells were incubated with medium containing [³⁵S]-methionine (10 µCi/µL; Perkin-Elmer) for 1 h at 37 °C. After labeling, cells were harvested, lysed by two freeze/thaw cycles, and analyzed by SDS/PAGE and autoradiography.

Antiviral Assays with Noninfluenza Viruses. The activity of the compounds against noninfluenza viruses was evaluated by PRAs for all viruses except COX B1. PRAs with HCMV AD169 were performed as described previously (20). For PRAs with HSV-1, Vero cells were seeded at 1.5×10^5 cells per well in 24-well plates. The next day, cells were infected with HSV-1 (strain F) at 80 pfu per well in DMEM for 1 h at 37 °C. For PRAs with AdV, A549 cells were seeded at 1×10^5 cells per well in 24-well plates. The next day, cells were infected with AdV at 40 pfu per well in DMEM for 1 h at 37 °C. For PRAs with VSV, L929 cells were seeded at 3×10^5 cells per well in 12-well plates, and the next day infected with VSV at 40 pfu per well in DMEM for 2 h at 37 °C. For PRAs with MV, Vero cells were seeded at 0.5×10^5 cells per well in 24-well plates, and the next day infected with MV at 40 pfu per well in DMEM for 2 h at 37 °C. For PRAs with RSV, HEp-2 cells were seeded at 1×10^5 cells per well in 24-well plates. The next day, cells were infected with RSV at 40 pfu per well in DMEM for 2 h at 37 °C. All infected cells were then incubated with medium containing 1.2% (wt/vol) Avicel cellulose, 2% (vol/vol) FBS, and various concentrations of each test compound. After appropriate periods of incubation, cell monolayers were fixed with 4% (vol/vol) formaldehyde and stained with 0.1% toluidine blue, and plaques were counted. The antiviral activity of the compounds against COX B1 was determined in Vero cells seeded at a density of 1×10^5 cells per well in 96-well plates by microscopic estimation of the cytopathic effect at 24 h p.i.

1. Cross S, Baroni M, Carosati E, Benedetti P, Clementi S (2010) FLAP: GRID molecular interaction fields in virtual screening. validation using the DUD data set. *J Chem Inf Model* 50:1442–1450.
2. Baroni M, Cruciani G, Sciabola S, Perruccio F, Mason JS (2007) A common reference framework for analyzing/comparing proteins and ligands. Fingerprints for Ligands and Proteins (FLAP): Theory and application. *J Chem Inf Model* 47:279–294.
3. Carosati E, et al. (2006) Calcium channel antagonists discovered by a multidisciplinary approach. *J Med Chem* 49:5206–5216.
4. Broccatelli F, et al. (2011) A novel approach for predicting P-glycoprotein (ABC B1) inhibition using molecular interaction fields. *J Med Chem* 54:1740–1751.
5. Brincat JP, et al. (2011) Discovery of novel inhibitors of the NorA multidrug transporter of *Staphylococcus aureus*. *J Med Chem* 54:354–365.
6. He X, et al. (2008) Crystal structure of the polymerase PA(C)-PB1(N) complex from an avian influenza H5N1 virus. *Nature* 454:1123–1126.
7. Carosati E, Sciabola S, Cruciani G (2004) Hydrogen bonding interactions of covalently bonded fluorine atoms: From crystallographic data to a new angular function in the GRID force field. *J Med Chem* 47:5114–5125.
8. von Itzstein M, et al. (1993) Rational design of potent sialidase-based inhibitors of influenza virus replication. *Nature* 363:418–423.
9. Crivori P, Cruciani G, Carrupt PA, Testa B (2000) Predicting blood-brain barrier permeation from three-dimensional molecular structure. *J Med Chem* 43:2204–2216.
10. Thompson JD, Higgins DG, Gibson TJ (1994) CLUSTAL W: Improving the sensitivity of progressive multiple sequence alignment through sequence weighting, position-specific gap penalties and weight matrix choice. *Nucleic Acids Res* 22:4673–4680.
11. Clamp M, Cuff J, Searle SM, Barton GJ (2004) The Jalview Java alignment editor. *Bioinformatics* 20:426–427.
12. Marti-Renom MA, et al. (2000) Comparative protein structure modeling of genes and genomes. *Annu Rev Biophys Biomol Struct* 29:291–325.
13. Fawell S, et al. (1994) Tat-mediated delivery of heterologous proteins into cells. *Proc Natl Acad Sci USA* 91:664–668.
14. Loregian A, et al. (2003) Inhibition of human cytomegalovirus DNA polymerase by C-terminal peptides from the UL54 subunit. *J Virol* 77:8336–8344.
15. Mullin AE, Dalton RM, Amorim MJ, Elton D, Digard P (2004) Increased amounts of the influenza virus nucleoprotein do not promote higher levels of viral genome replication. *J Gen Virol* 85:3689–3698.
16. Benfield CT, Lyall JW, Kochs G, Tiley LS (2008) Asparagine 631 variants of the chicken Mx protein do not inhibit influenza virus replication in primary chicken embryo fibroblasts or in vitro surrogate assays. *J Virol* 82:7533–7539.
17. Jackson D, Cadman A, Zurcher T, Barclay WS (2002) A reverse genetics approach for recovery of recombinant influenza B viruses entirely from cDNA. *J Virol* 76:11744–11747.
18. Fodor E, Smith M (2004) The PA subunit is required for efficient nuclear accumulation of the PB1 subunit of the influenza A virus RNA polymerase complex. *J Virol* 78:9144–9153.
19. Loregian A, Appleton BA, Hogle JM, Coen DM (2004) Residues of human cytomegalovirus DNA polymerase catalytic subunit UL54 that are necessary and sufficient for interaction with the accessory protein UL44. *J Virol* 78:158–167.
20. Loregian A, Coen DM (2006) Selective anti-cytomegalovirus compounds discovered by screening for inhibitors of subunit interactions of the viral polymerase. *Chem Biol* 13:191–200.
21. Blok V, et al. (1996) Inhibition of the influenza virus RNA-dependent RNA polymerase by antisera directed against the carboxy-terminal region of the PB2 subunit. *J Gen Virol* 77:1025–1033.

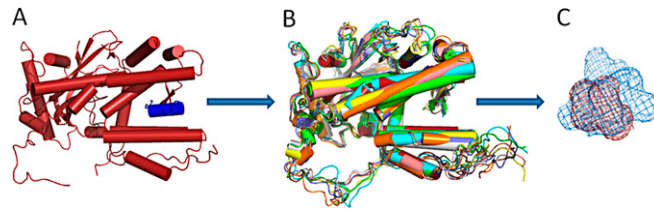


Fig. S1. Modeling of the PA subunit. (A) Crystal structure of the PA (in red)–PB1 (in blue) complex (PDB code 3CM8). (B) Alignment of the six PA conformations generated by molecular dynamics simulations on the PA crystal structure template. (C) Comparative analysis of the cavities in PA binding site obtained from molecular dynamics simulations. The largest and the smallest volumes detected are reported in dark-red and blue colors, respectively. The smallest volume refers to the PA crystal structure template.

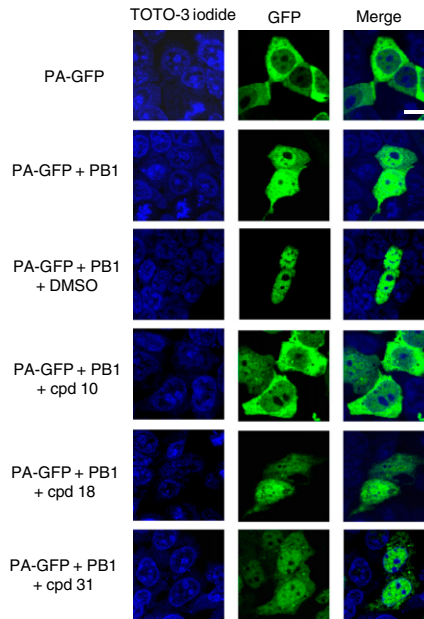


Fig. S2. Effect of test compounds on intranuclear localization of the PA–PB1 complex. HEK 293T cells were transfected with plasmids expressing PB1 and a PA–GFP fusion protein in the presence of test compounds or DMSO as a control. Cells transfected with the PA–GFP–expressing plasmid alone served as a negative control. 24 h posttransfection, cells were examined by confocal laser scanning microscopy. Individual green (GFP) and blue (TOTO-3 iodide) channels and merged images are shown. (Scale bar, 5 μm .)

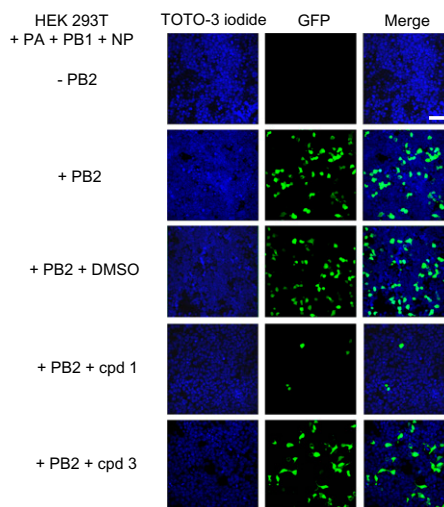


Fig. S3. Activities of the compounds in FluB virus minireplicon assays. HEK 293T cells were transfected with plasmids encoding PB1, PB2, PA, and NP of FluB, and with a plasmid containing a GFP reporter gene flanked by noncoding sequences of FluB virus genome. GFP expression was examined at 24 h posttransfection by confocal laser microscopy. The green (GFP) and blue (TOTO-3 iodide) channels are shown; merged images of the green and blue channels are shown on the right. (Scale bar, 35 μm .)

Table S1. Inhibitory activity of the test compounds on FluA virus PA–PB1 interaction or on human cytomegalovirus UL54–UL44 interaction

Compound	Inhibition of PA–PB1 interaction at 50 μ M	Inhibition of UL54–UL44 interaction at 50 μ M	Inhibition of PA–PB1 interaction (IC ₅₀ , μ M)
1	+	–	30.4 \pm 4.5
2	–	\pm	ND
3	–	–	ND
4	\pm	–	ND
5	+	–	25.4 \pm 3.9
6	\pm	–	ND
7	–	–	ND
8	+	–	>200
9	\pm	–	ND
10	+	–	90.7 \pm 2.4
11	\pm	–	ND
12	+	–	20.1 \pm 3.2
13	–	–	ND
14	–	\pm	ND
15	–	–	ND
16	–	–	ND
17	–	–	ND
18	+	–	199.5 \pm 5.3
19	–	–	ND
20	\pm	–	ND
21	\pm	–	ND
22	\pm	–	ND
23	–	\pm	ND
24	–	–	ND
25	–	–	ND
26	–	–	ND
27	–	–	ND
28	–	\pm	ND
29	–	–	ND
30	–	–	ND
31	+	–	170.6 \pm 4.7
32	–	–	ND
PB1 _{1–15} –Tat peptide	+	–	35.5 \pm 3.1

+, inhibition of interaction; \pm , weak inhibition of interaction; –, no inhibition of interaction; IC₅₀, concentration of the compound that inhibits 50% of PA–PB1 interaction; ND, not determined.

Table S2. Cytotoxicity of most active compounds

Compound	CC ₅₀ , μ M						
	HEK 293T	MDCK	A549	L929	Vero	HFF	Hep-2
1	>1,000	>1,000	>250	>250	>250	>250	>250
3	>250	>250	>250	>250	>250	>250	>250
5	>1,000	>1,000	>250	>250	>250	>250	>250
10	>250	>250	ND	ND	ND	ND	ND
12	2.4 \pm 1.7	12.5 \pm 3.2	ND	ND	ND	ND	ND
18	225.6 \pm 7.8	>250	ND	ND	ND	ND	ND
31	>250	>250	ND	ND	ND	ND	ND
PB1 _{1–15} –Tat peptide	>250	>250	>250	ND	ND	ND	ND
RBV	ND	>250	ND	>250	>250	ND	>250
Oseltamivir	>250	>250	>250	ND	>250	ND	ND

CC₅₀, concentration of the compound that produces 50% cytotoxicity as determined by MTT assays; ND, not determined; RBV, ribavirin. Reported values represent the means \pm SD of data derived from at least three independent experiments.

Table S3. Effects of selected compounds on the replication of FluA viruses

Virus subtype and strain	Compound activity (ED ₅₀ , μM)						
	1	3	5	AL5	RBV	Osetamivir	Amantadine
A (H1N1)							
A/PR/8/34	18.6 ± 4.1	>100	>100	>100	8.4 ± 2.3	0.01 ± 0.004	>100
A/Solomon Island/3/06	12.2 ± 2.6	>100	>100	>100	15.2 ± 4.1	ND	5.5 ± 1.2
A/Roma-ISS/2/08	17.3 ± 3.7	>100	>100	>100	15.3 ± 3.7	ND	ND
A/California/7/09	19.1 ± 4.3	>100	75.5 ± 8.8	>100	16.4 ± 2.8	ND	ND
A/Padova/30/2011	15.5 ± 3.6	>100	>100	>100	13.3 ± 3.5	ND	ND
A/Padova/72/2011	20.0 ± 2.9	>100	>100	>100	15.7 ± 4.4	ND	ND
A/Padova/253/2011	18.2 ± 5.2	>100	>100	>100	17.2 ± 4.7	ND	ND
A/Parma/24/09 (oseltamivir resistant)	22.5 ± 3.7	>100	82.2 ± 10.3	>100	18.6 ± 2.9	>100	ND
A (H3N2)							
A/Wisconsin/67/05	22.5 ± 3.2	>100	>100	>100	17.5 ± 3.5	ND	ND

ED₅₀, concentration of the compound that inhibits 50% of plaque formation; ND, not determined; RBV, ribavirin.

Table S4. Effects of selected compounds on the replication of FluB viruses

Virus strain	Compound activity (ED ₅₀ , μM)				
	1	3	5	AL5	RBV
B/Lee/40	14.5 ± 3.5	>100	>100	>100	20.2 ± 3.4
B/Malaysia/2506/04	12.5 ± 2.2	>100	>100	>100	17.5 ± 3.4
B/Bangladesh/333/07	14.3 ± 4.3	>100	>100	>100	14.3 ± 5.1
B/Brisbane/60/08	19.6 ± 3.1	>100	>100	>100	16.6 ± 5.6
B/Padova/2/2011	16.5 ± 5.6	>100	>100	>100	19.1 ± 6.4
B/Padova/3/2011	19.2 ± 3.2	>100	>100	>100	17.7 ± 3.8
B/Padova/42/2011	21.0 ± 2.8	>100	>100	>100	20.0 ± 4.7

ED₅₀, concentration of the compound that inhibits 50% of plaque formation; RBV, ribavirin.

Table S5. Activities of test compounds against other RNA and DNA viruses

Virus	Family	Genome	Compound activity (ED ₅₀ , μM)				
			1	3	5	RBV	GCV
HSV-1	<i>Herpesviridae</i>	dsDNA	>100	>100	>100		0.1 ± 0.04
HCMV	<i>Herpesviridae</i>	dsDNA	>100	>100	>100		1.2 ± 1.3
AdV	<i>Adenoviridae</i>	dsDNA	>100	>100	>100		
COX B1	<i>Picornaviridae</i>	(+) ssRNA	>100	>100	>100		
VSV	<i>Rhabdoviridae</i>	(-) ssRNA	>100	>100	>100	10.3 ± 2.9	
MV	<i>Paramyxoviridae</i>	(-) ssRNA	>100	>100	>100		
RSV	<i>Paramyxoviridae</i>	(-) ssRNA	>100	>100	>100	21.6 ± 3.6	

AdV, adenovirus; COX B1, coxsackie virus B1; ds, double stranded; ED₅₀, concentration of the compound that inhibits 50% of plaque formation or cytopathic effect; GCV, ganciclovir; HCMV, human cytomegalovirus; HSV-1, herpes simplex virus type 1; MV, measles virus; RBV, ribavirin; RSV, respiratory syncytial virus; ss, single stranded; VSV, vesicular stomatitis virus.